

# Theoretical Study of the Electrostatic Lens Aberrations of a Negative Ion Accelerator for a Neutral Beam Injector

Kenji MIYAMOTO and Akiyoshi HATAYAMA<sup>1)</sup>

*Naruto University of Education, 748 Nakashima, Takashima, Naruto-cho, Naruto-shi,  
Tokushima 772-8502, Japan*

<sup>1)</sup>*Faculty of Science and Technology, Keio University, 3-14-1 Hiyoshi, Kohoku-ku, Yokohama 223-8522, Japan*

(Received 25 July 2008 / Accepted 21 December 2008)

Aberrations due to the electrostatic lenses of a negative ion accelerator for a neutral beam injector and the space charge effect are theoretically investigated. A multi-stage extractor/accelerator is modeled and the aberration coefficients are numerically calculated using the eikonal method, which is conventionally used in electron optics. The aberrations are compared with the radii of a beam core with good beam divergence and a beam halo with poor beam divergence.  $H^-$  beamlet profile measurements give the  $1/e$  radii of the beam core and beam halo of 5.8 mm (beam divergence angle: 6 mrad) and 11.5 mm (beam divergence angle: 12 mrad), respectively. When the beam divergence angle of the beam core is 5 mrad and the beam energy is 406 keV, the aberrations due to the electrostatic lenses are less than a few millimeters, thus are less than the radii of the beam core and beam halo. The geometrical aberrations due to the space charge effect (negative ion current density: 10 mA/cm<sup>2</sup>), however, are estimated to be much larger than the radius of the beam halo. Although the aperture radii of the grids are not taken into account in this estimation, the results indicate that the space charge effect is an important factor in the aberration or beam halo in a negative ion accelerator.

© 2009 The Japan Society of Plasma Science and Nuclear Fusion Research

Keywords: nuclear fusion device, NBI, accelerator, negative ion beam, aberration, electrostatic lens

DOI: 10.1585/pfr.4.007

## 1. Introduction

A negative ion-based neutral beam injection system (N-NBI system) is a promising candidate for plasma heating and current drive of fusion reactors such as the international thermonuclear experimental reactor (ITER). ITER requires the N-NBI system to provide high power neutral beams with a beam energy of 1 MeV and beam power of 50 MW using three injectors [1–4].

A negative ion source/accelerator that can produce negative ion beams with high current and power is the key component for the N-NBI system. Negative ion beams with a beam energy of 1 MeV, beam current of 40 A, and beam current density of 20 mA/cm<sup>2</sup> are required for the ITER-NBI [1–4]. To suppress the geometrical loss of negative ion beams and heat loads in the beamline, NB duct, and injection port, it is essential to accelerate the negative ion beams with good beam optics.

As for the  $H^-$  beam optics, Holmes et al. measured the  $H^-$  ion beamlet produced with a pure volume source, and reported that the profile consists of two Gaussian portions—a beam core with good divergence and a beam halo with poor divergence [5].  $H^-$  ion beamlet profiles with these two Gaussian portions were confirmed with the 400 keV negative ion accelerator [6, 7]. In the ITER-NBI, the beamlet is also considered to consist of the beam core

(< 5 mrad) and beam halo (> 15 mrad), and the ITER-NBI is designed on the basis that the power fraction of the beam halo is estimated to be 15% of the total beam power [8].

It is well known that the effects of aberrations degrade the charged particle beam optics. Generating aberrations is inevitable when the charged particle beams are extracted, accelerated, transmitted, and focused with electrostatic and magnetic fields. For charged particle optical instruments in the field of the electron microscopes and focused ion beam systems, aberrations degrade the focused beam spot, limiting the spatial resolution of these instruments. Therefore, in developing of the charged particle optical instruments, many authors have studied the aberrations due to the electrostatic lens, magnetic lens, and space charge effect [9–17].

In the ITER-NBI design, there is no specification for an acceptable level of aberration. However, very little is known about the aberrations in the negative ion source/accelerator for the N-NBI system. In fact, the aberrations arise from the electrostatic lenses, magnetic lenses produced by the magnetic filter and permanent magnets for electron suppression, the plasma-beam boundary, and the space charge effect. Moreover, the aberrations are considered to be one of the reasons for the beam halo. As described above, although the beam halo was verified experimentally in the  $H^-$  beamlet profile [5–7], its physical

author's e-mail: kmiyamot@naruto-u.ac.jp

mechanism is not clear.

The main purpose of the present study is to investigate the aberrations in the extractor/accelerator theoretically. This paper focuses on aberrations due to the electrostatic lenses and the space charge effect. The well-known eikonal method [17–21] is used to calculate these aberrations, and the calculated aberrations are discussed quantitatively by comparing them with the radii of the beam core and beam halo, as reported in Refs. [6, 7].

This article is constructed as follows: the calculation models for the electrostatic potential, negative ion beam trajectory, and aberration are described in Sec. 2; the calculation results are shown and discussed in Sec. 3; and a summary is given in Sec. 4.

## 2. Calculation Model

Figure 1 shows a cross-sectional view of the extractor and accelerator for the present model. Figure 1 (a) shows an overall view of the extractor and accelerator and Fig. 1 (b) shows a magnified view of the extractor. The extractor and accelerator are multi-aperture and multi-stage types. Negative ions are extracted and accelerated electrostatically.

The extractor consists of a plasma grid (PG) and an extraction grid (EXG), which have the same structure as the extractor of the negative ion source for ITER-NBI. In order to extract negative ions with good beam optics, the PG and EXG are shaped to produce convergent electrostatic lenses in the extractor. Permanent magnets are embedded in the EXG to suppress the electrons extracted along with negative ions. These magnets produce the magnetic lens. In the present model, this magnetic lens is not taken into account.

The accelerator consists of a first acceleration grid (A1G), second acceleration grid (A2G), and grounded grid

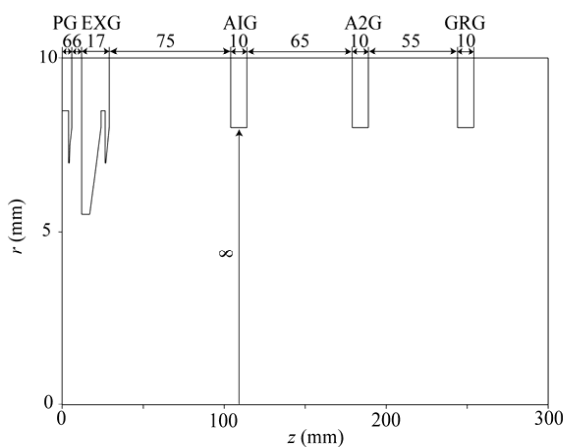


Fig. 1 Cross-sectional view of the extractor and accelerator in the present model. (a) Overall view of the extractor and accelerator. (b) A magnified view of the extractor.

(GRG). The aperture diameter, gap length, and number of acceleration stages are the same as those of the accelerators for JT-60U N-NBI [22, 23] and the 400 keV negative ion source [24, 25]. The gap length is designed to be progressively shorter in the downstream stages to form converging electrostatic lenses at each grid aperture, and thereby suppress beam divergence due to the space charge effect.

### 2.1 Calculation of electric field

To calculate the electric field in the extractor and accelerator, Laplace's equation is solved using a finite difference method with successive over-relaxation.

1) The extractor and accelerator are modeled to be rotationally symmetric. The  $r$ -axis is taken to be the direction of the beam radius, whereas the  $z$ -axis is taken to be the direction of beam acceleration.

2) The mesh sizes are 0.025, 0.05, 0.1, and 0.2 mm. The minimum mesh size of 0.025 mm is approximately the Debye length  $\lambda_D$  in the extraction region of the negative ion source. The Debye length  $\lambda_D$  can be estimated as follows: at an arc power of 10 kW, the ion saturation current in the extraction region is approximately 200 A/m<sup>2</sup> [26, 27]. Assuming that the electron temperature  $T_e$  is 1 eV, and the ratio of the electron density to the ion density is 0.9 [28], one obtains

$$n_e = 0.9 \times \frac{200}{1.60 \times 10^{-19} \times \exp(-0.5) \times \sqrt{1.60 \times 10^{-19} \times 1 / 1.67 \times 10^{-27}}} = 1.9 \times 10^{17} \text{ m}^{-3}.$$

Therefore,  $\lambda_D$  is estimated to be 0.017 mm.

3) The entrance of the PG is set to be  $z = 0$  mm. The position where the negative ion beamlet profiles was measured, as in Refs. [6, 7], corresponds to  $z = 1214$  mm in the present model. Modeling to this position incurs high calculation costs. Since an electric field generally penetrates into the field-free region by a distance of the diameter of an aperture (at most), the calculation region is modeled up to  $z = 270$  mm, i.e., 16 mm downstream from the GRG exit. The regions of  $z > 270$  mm are assumed to be field-free ( $\mathbf{E} = 0$ ).

4) The plasma-ion boundary is equivalent to an object plane  $z = z_0$ . Except for the electrodes, the mesh regions of  $z \leq z_0 - dh$  are assumed to be the plasma region, and the electrostatic potential is set to be zero.

5) The shape of the plasma-beam boundary will result in the aberrations because the plasma-beam boundary has a lens effect [29]. In the present model, the plasma-beam boundary is assumed to be flat. Thus, aberrations caused by the shape of the plasma-beam boundary are not considered. An example of equipotentials in the extractor is shown in Fig. 2.

6) In the experiment, the GRG is grounded [6, 7]; however, the PG is grounded in the present model. The grid voltages are modeled to be optically optimized at a beam energy

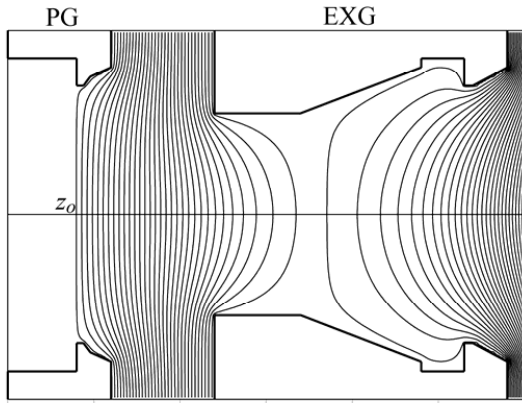


Fig. 2 Example of equipotentials in the extractor.

Table 1 Voltages of each grid in the extractor and accelerator.

Grid	PG	EXG	A1G	A2G	GRG
Voltage (kV)	0	6.40	139.73	273.07	406.40

of 406 keV, as shown in Table 1. The electrostatic lenses in the present model are similar to those of the 400 keV negative ion accelerator.

## 2.2 Calculation of ion beamlet trajectory

The paraxial ray equation of the negative ion beamlet is given by [15]

$$u''_G + \frac{\phi'}{2\phi} u'_G + \frac{\phi'' + \rho}{4\phi} u_G = 0, \quad (1)$$

where  $\phi$  is an electrostatic potential, and  $\rho$  is the space charge density for the  $H^-$  ion beamlet. In Eq. (1), primes signify differentiation with respect to  $z$ . The paraxial ray equation is solved using the fourth-order Runge-Kutta method.

The two fundamental solutions of Eq. (1) are given as  $g = g(z)$  ( $g$ -trajectory) and  $h = h(z)$  ( $h$ -trajectory) with the following initial conditions at the object plane  $z = z_0$ :

$$g(z_0) = 1, \quad g'(z_0) = 0, \quad h(z_0) = 0, \quad h'(z_0) = 1. \quad (2)$$

The solution of the paraxial ray Eq. (1) is given by

$$u_G = A_1 g(z) + A_2 h(z), \quad (3)$$

where  $A_1$  and  $A_2$  are the constants.

In general, the optical properties of the electrostatic lenses can be evaluated from the  $g$ -trajectory and  $h$ -trajectory (see Fig. 3):

- The position of an image plane  $z = z_i$  is estimated from  $h(z_i) = 0$ .
- Magnification  $M$  is defined by  $g(z_i) = |M|$ .

- Focal length  $f_i$  is given by  $f_i = -\frac{1}{g'(z_i)}$ .
- The position of a focal plane  $z = z_{F_i}$  is given by  $z_{F_i} = z_i + M f_i$ .
- The position of a principal plane  $z = z_{h_i}$  is given by  $z_{h_i} = z_{F_i} - f_i$ .

Moreover, the aberration due the electrostatic lenses and the space charge effect can be estimated with the two fundamental solutions, as will be shown in the next section.

## 2.3 Estimation of aberration due to the electrostatic lenses

The aberration of the electrostatic lenses is calculated using the eikonal method, which is conventionally used in electron optics [17–21]. As the high order derivatives such as  $\phi^{(3)}$  and  $\phi^{(4)}$  cause inaccuracies in numerical integration, these high order derivatives are excluded using Seaman's procedure [30–32].

The space charge effect is not taken into account in the following.

### 2.3.1 Geometrical aberration

From the eikonal method (see Appendix), the geometrical aberration  $u_3(z_i)$  referred to the object side is given as

$$u_3(z_i) = M \left( C_s^{(o)} u_o'^2 \bar{u}_o' + C_1^{(o)} u_o' \bar{u}_o' u_o + C_r^{(o)} u_o'^2 \bar{u}_o + C_a^{(o)} u_o^2 \bar{u}_o' + C_f^{(o)} u_o \bar{u}_o u_o' + C_d^{(o)} u_o^2 \bar{u}_o \right), \quad (4)$$

In Eq. (4), the aberration is expressed in terms of the beam trajectory and beam divergence angle at the object plane, i.e.,  $u_G(z_0) = u_o$ ,  $u'_G(z_0) = u_o'$ . Moreover,  $\bar{u}_o$  and  $\bar{u}_o'$  are the complex conjugates of  $u_o$  and  $u_o'$ , respectively. The geometrical aberration coefficients of  $C_s^{(o)}$ ,  $C_1^{(o)}$ ,  $C_r^{(o)}$ ,  $C_a^{(o)}$ ,  $C_f^{(o)}$ ,  $C_d^{(o)}$  are defined as follows:

$C_s^{(o)}$ : a coefficient of spherical aberration

$C_1^{(o)}$ ,  $C_r^{(o)}$ : a coefficient of coma

$C_a^{(o)}$ : a coefficient of stigmatism

$C_f^{(o)}$ : a coefficient of field curvature

$C_d^{(o)}$ : a coefficient of distortion

In terms of  $g(z)$  and  $h(z)$ , the aberration coefficients of  $C_s^{(o)}$ ,  $C_1^{(o)}$ ,  $C_r^{(o)}$ ,  $C_a^{(o)}$ ,  $C_f^{(o)}$ ,  $C_d^{(o)}$  are given as follows:

$$C_s^{(o)} = \frac{1}{32} \int_{z_0}^{z_i} \sqrt{\frac{\phi}{\phi_0}} \{ F_1 h^4 + F_2 h^3 h' + F_3 h^2 h'^2 \} dz - \frac{1}{32} \sqrt{\frac{\phi}{\phi_0}} [ E_1 h^4 + E_2 h^3 h' + E_3 h^2 h'^2 + E_5 h h'^3 ]_{z_0}^{z_i},$$

$$\frac{1}{2} C_1^{(o)} = C_r^{(o)} = \frac{1}{128} \int_{z_0}^{z_i} \sqrt{\frac{\phi}{\phi_0}} \{ 4 F_1 g h^3 + F_2 h^2 (2g'h + (gh)') + 2 F_3 h h' (gh)' \} dz - \frac{1}{128} \sqrt{\frac{\phi}{\phi_0}} [ 4 E_1 g h^3 + E_2 h^2 (2g'h + (gh)') + 2 E_3 h h' (gh)' + E_5 h'^2 (2gh' + (gh)') ]_{z_0}^{z_i},$$

$$\begin{aligned}
 C_a^{(o)} &= \frac{1}{64} \int_{z_o}^{z_i} \sqrt{\frac{\phi}{\phi_o}} \{2F_1 g^2 h^2 - F_2 g g'(gh)' + 2F_3 g h g' h'\} dz \\
 &\quad - \frac{I^2}{128 \sqrt{\phi_o}} \int_{z_o}^{z_i} \frac{F_4}{\sqrt{\phi}} dz - \frac{1}{64} \sqrt{\frac{\phi}{\phi_o}} [2E_1 g^2 h^2 \\
 &\quad + E_2 g h (gh)' + 2E_3 g h g' h' + E_5 g' h' (gh)']_{z_o}^{z_i}, \\
 C_f^{(o)} &= \frac{1}{64} \int_{z_o}^{z_i} \sqrt{\frac{\phi}{\phi_o}} \{4F_1 g^2 h^2 + 2F_2 g h (gh)' + F_3 (gh)^2\} dz \\
 &\quad - \frac{I^2}{128 \sqrt{\phi_o}} \int_{z_o}^{z_i} \frac{F_4}{\sqrt{\phi}} dz - \frac{1}{64} \sqrt{\frac{\phi}{\phi_o}} [4E_1 g^2 h^2 \\
 &\quad + E_2 g h (gh)' + E_3 (gh)^2 + 2E_5 g' h' (gh)']_{z_o}^{z_i}, \\
 C_d^{(o)} &= \frac{1}{128} \int_{z_o}^{z_i} \sqrt{\frac{\phi}{\phi_o}} \{4F_1 g^3 h + F_2 g^2 (2g' h + (gh)') \\
 &\quad + 2F_3 g g' (gh)'\} dz - \frac{1}{128} \sqrt{\frac{\phi}{\phi_o}} [4E_1 g^3 h + E_2 g^2 (2g' h \\
 &\quad + (gh)') + 2E_3 g g' (gh)' + E_5 g'^2 (2g h' + (gh)')]_{z_o}^{z_i}, \tag{5}
 \end{aligned}$$

where

$$\begin{aligned}
 I &= \sqrt{\phi} (gh' - g'h), \\
 E_1 &= \frac{1}{2} \frac{\phi' \phi''}{\phi^2} + \phi^{(3)}, \\
 E_2 &= -\frac{4\phi''}{\phi}, \\
 E_3 &= -\frac{8\phi'}{\phi}, \\
 E_5 &= -16, \\
 F_1 &= -\frac{3}{4} \frac{\phi'^2 \phi''}{\phi^3} + \frac{5}{2} \left(\frac{\phi''}{\phi}\right)^2, \\
 F_2 &= \frac{10\phi' \phi''}{\phi^2}, \\
 F_3 &= 12 \left(\frac{\phi'}{\phi}\right)^2. \tag{6}
 \end{aligned}$$

On the other hand, the geometrical aberration  $u_3(z_i)$  referred to the image side is given as

$$\begin{aligned}
 u_3(z_i) &= C_s^{(i)} u_i'^2 \bar{u}_i' + C_1^{(i)} u_i' \bar{u}_i' u_i + C_r^{(i)} u_i'^2 \bar{u}_i + C_a^{(i)} u_i^2 \bar{u}_i' \\
 &\quad + C_f^{(i)} u_i \bar{u}_i u_i' + C_d^{(i)} u_i^2. \tag{7}
 \end{aligned}$$

In this case, the aberrations are expressed in terms of the beam trajectory and beam divergence angle at the image plane, i.e.,  $u_G(z_i) = u_i$ ,  $u_G'(z_i) = u_i'$ . Moreover,  $\bar{u}_i$  and  $\bar{u}_i'$  are the complex conjugates of  $u_i$  and  $u_i'$ , respectively.

The relation between the aberration coefficients in Eqs. (4) and (7) is given by

$$\begin{aligned}
 C_s^{(i)} &= M^4 \xi_1^3 C_s^{(o)}, \\
 C_1^{(i)} &= 2M^2 \xi_1^2 \left\{ \frac{M}{f_o} C_s^{(o)} + C_r^{(o)} \right\}, \\
 C_r^{(i)} &= M^2 \xi_1^2 \left\{ \frac{M}{f_o} C_s^{(o)} + C_r^{(o)} \right\}, \\
 C_a^{(i)} &= \xi_1 \left\{ C_a^{(o)} + \frac{2MC_r^{(o)}}{f_o} + \frac{M^2}{f_o^2} C_s^{(o)} \right\},
 \end{aligned}$$

$$\begin{aligned}
 C_f^{(i)} &= \xi_1 \left\{ C_f^{(o)} + \frac{4MC_r^{(o)}}{f_o} + \frac{2M^2}{f_o^2} C_s^{(o)} \right\}, \\
 C_d^{(i)} &= \frac{1}{M^2} C_d^{(o)} + \frac{1}{Mf_o} (C_f^{(o)} + C_a^{(o)}) + \frac{3C_r^{(o)}}{f_o^2} + \frac{MC_s^{(o)}}{f_o^3}, \tag{8}
 \end{aligned}$$

where

$$\xi_i = \sqrt{\frac{\phi_i}{\phi_o}}, \quad \phi_o = \phi(z_o), \quad \phi_i = \phi(z_i). \tag{9}$$

In Eq. (8),  $f_o$  is the focal length on the object side.

### 2.3.2 Chromatic aberration

From the eikonal method, the chromatic aberration  $u_c(z_i)$  referred to the object side is given as

$$u_c(z_i) = -M (C_c^{(o)} u_o' + C_m^{(o)} u_o) \frac{\Delta\phi}{\phi_i}, \tag{10}$$

where  $e\Delta\phi$  is the deviation of initial kinetic energy. In Eq. (10),  $C_c^{(o)}$  and  $C_m^{(o)}$  are the coefficients of an axial chromatic aberration and chromatic aberration of magnification, respectively. These coefficients are given as

$$\begin{aligned}
 C_c^{(o)} &= \frac{3}{8} \int_{z_o}^{z_i} \sqrt{\frac{\phi_o}{\phi}} \left(\frac{\phi'}{\phi}\right)^2 h^2 dz, \\
 C_m^{(o)} &= \frac{3}{8} \int_{z_o}^{z_i} \sqrt{\frac{\phi_o}{\phi}} \left(\frac{\phi'}{\phi}\right)^2 gh dz + \frac{1}{4} \left(\frac{\phi_o}{\phi_i} - 1\right). \tag{11}
 \end{aligned}$$

On the other hand, the chromatic aberration  $u_c(z_i)$  referred to the image side is given as

$$u_c(z_i) = - (C_c^{(i)} u_i' + C_m^{(i)} u_i) \frac{\Delta\phi}{\phi_i}. \tag{12}$$

These aberration coefficients  $C_c^{(i)}$ ,  $C_m^{(i)}$  are given as

$$\begin{aligned}
 C_c^{(i)} &= M^2 \xi_1^3 C_c^{(o)}, \\
 C_m^{(i)} &= \xi_1^2 \left\{ C_m^{(o)} + \frac{M}{f_o} C_c^{(o)} \right\}. \tag{13}
 \end{aligned}$$

### 2.3.3 Aberration coefficients with length

The position where the negative ion beamlet profile is measured corresponds to the image plane. Thus, to compare the calculation results with the experimental results in Refs. [6, 7], it is convenient to express the aberration in terms of the beam trajectory and beam divergence angle at the image plane. From Eqs. (7) and (12), the aberrations at the image plane can be given as

$$\begin{aligned}
 \Delta u(z_i) &= C_s^{(i)} u_i'^2 \bar{u}_i' + C_1^{(i)} u_i' \bar{u}_i' u_i + C_r^{(i)} u_i'^2 \bar{u}_i + C_a^{(i)} u_i^2 \bar{u}_i' \\
 &\quad + C_f^{(i)} u_i \bar{u}_i u_i' + C_d^{(i)} u_i^2 \bar{u}_i - (C_c^{(i)} u_i' + C_m^{(i)} u_i) \frac{\Delta\phi}{\phi_i}. \tag{14}
 \end{aligned}$$

The aberration coefficients in Eq. (14) differ in their dimensions. Using  $s_i$ , which is the distance between a principle plane  $z_{hi}$  and the image plane  $z_i$ , as shown in Fig. 3,

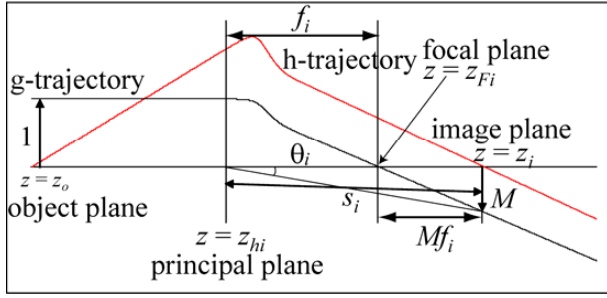


Fig. 3 Diagram of the two fundamental paraxial trajectories.

the aberration coefficients can be expressed as those with the dimension of length as follows:

$$\Delta u(z_i) = c_s^{(i)} u_i'^2 \bar{u}_i' + c_1^{(i)} u_i' \bar{u}_i' \theta_i + c_r^{(i)} u_i'^2 \bar{\theta}_i + c_a^{(i)} \bar{u}_i' \theta_i^2 + c_f^{(i)} u_i' \theta_i \bar{\theta}_i + c_d^{(i)} \theta_i^2 \bar{\theta}_i - (c_c^{(i)} u_i' + c_m^{(i)} \theta_i) \frac{\Delta \phi}{\phi_i}, \quad (15)$$

where

$$\begin{aligned} c_s^{(i)} &= C_c^{(i)}, & c_1^{(i)} &= C_1^{(i)} s_i, & c_r^{(i)} &= C_r^{(i)} s_i, & c_a^{(i)} &= C_a^{(i)} s_i^2, \\ c_f^{(i)} &= C_f^{(i)} s_i^2, & c_d^{(i)} &= C_d^{(i)} s_i^3, & c_c^{(i)} &= C_c^{(i)}, & c_m^{(i)} &= C_m^{(i)} s_i. \end{aligned} \quad (16)$$

In Eq. (15),  $\theta_i$  is an angle defined in Fig. 3, and  $\bar{\theta}_i$  is the complex conjugate of  $\theta_i$ . In Sec. 3, the aberration due to the electrostatic lenses is calculated using Eqs. (15) and (16).

## 2.4 Estimation of aberration due to the space charge effect

The geometrical aberration coefficients due to the space charge effect are given as follows [17]:

- a coefficient of spherical aberration

$$C_s S^{(o)} = \frac{1}{4\epsilon_0} \int_{z_o}^{z_i} \frac{\rho(z)}{\phi(z)} h^2 h'^2 dz, \quad (17)$$

- a coefficient of coma

$$C_{lr} S^{(o)} = \frac{1}{8\epsilon_0} \int_{z_o}^{z_i} \frac{\rho(z)}{\phi(z)} (h^2 g' h' + g h h'^2) dz, \quad (18)$$

- a coefficient of stigmatism

$$C_a S^{(o)} = \frac{1}{4\epsilon_0} \int_{z_o}^{z_i} \frac{\rho(z)}{\phi(z)} h g h' g' dz, \quad (19)$$

- a coefficient of field curvature

$$C_f S^{(o)} = \frac{1}{4\epsilon_0} \int_{z_o}^{z_i} \frac{\rho(z)}{\phi(z)} (h g' + g h')^2 dz, \quad (20)$$

- a coefficient of distortion

$$C_d S^{(o)} = \frac{1}{4\epsilon_0} \int_{z_o}^{z_i} \frac{\rho(z)}{\phi(z)} (g h g'^2 + g^2 g' h') dz. \quad (21)$$

In Eqs. (17)–(21),  $\rho(z)$  is a space charge density for H<sup>-</sup> ion beamlet given by

$$\rho(z) = \frac{I}{\pi R(z)^2 v_z(z)}, \quad (22)$$

where  $I$  is the total current,  $R(z)$  is the beamlet radius, and  $v_z(z)$  is the velocity component parallel to the  $z$ -axis. The beamlet radius  $R(z)$  can be expressed by the relation

$$R(z) = R_o g(z) + \alpha_o h(z), \quad (23)$$

where  $R_o$  and  $\alpha_o$  are the beamlet radius and incident angle at the object plane, respectively.

These aberration coefficients are referred to the object side. Equation (8) transforms these aberration coefficients into the aberration coefficients referred to the image side.

## 3. Result and Discussion

### 3.1 Dependence of aberration coefficients on object planes

Before estimating the aberration due to the electrostatic lenses, the dependence of the aberration coefficients on the position of the object planes is investigated. The aberration coefficients referred to the object side  $C^{(o)}$  (given by Eqs. (5) and (11)) are shown in Fig. 4 as a function of the object planes  $z_o$ . On the other hand, the aberration coefficients referred to the image side  $C^{(i)}$  (given by Eqs. (8) and (13)) are shown in Fig. 5 as a function of the object planes  $z_o$ . In Fig. 5, the aberration coefficients  $C^{(i)}$  are shown in a log scale. These aberration coefficients are normalized by the values at  $z_o = 1$  mm. The mesh size is 0.1 mm.

Figures 4 and 5 show that the aberration coefficients  $C^{(i)}$  vary with  $z_o$  larger than the aberration coefficients  $C^{(o)}$ , except for the aberration coefficients of distortion  $C_d^{(i)}$ . For  $z_o \geq 2.5$  mm, the aberration coefficients  $C^{(i)}$  increase monotonically with  $z_o$ .

The reason  $C^{(o)}$  and  $C^{(i)}$  increase with  $z_o$  can be qualitatively explained as follows: As  $z_o$  is closer to the entrance of the PG (or the negative ion source), the negative ion beams are affected significantly by the penetrating field in the PG. The penetrating field causes the negative ion beams to converge to the beam axis. Therefore, the negative ion beams starting from the larger  $z_o$  can pass the locations peripheral to the aperture, and then are more heavily influenced by the fringe field to aberration. This can be confirmed by comparing the  $h$ -trajectory for  $z_o = 1.0$  mm with that for  $z_o = 4.5$  mm, as shown in Fig. 6.

Note that the  $h$ -trajectory starting from  $z_o = 1.0$  mm diverges after passing the location of  $z = z_i$ . However, this diverging trajectory does not contribute to aberration because the integration of aberration coefficients is performed in the range from  $z = z_o$  to  $z = z_i$  (see Eqs. (5) and (11)).

The positions of the image planes  $z_i$  are shown in Fig. 7 as a function of  $z_o$ . As the position of object plane

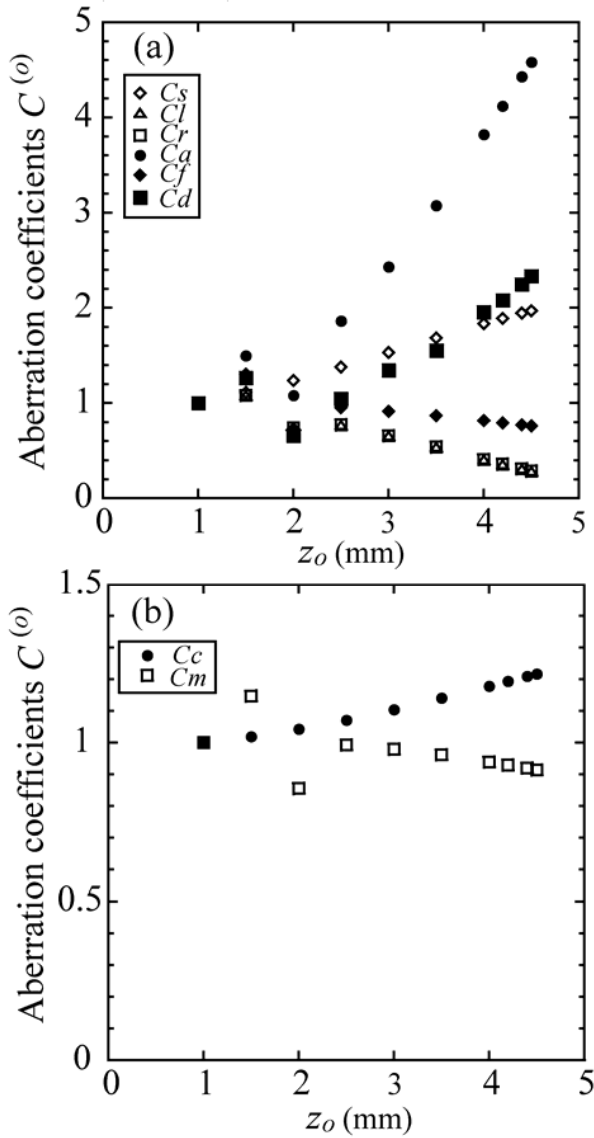


Fig. 4 Aberration coefficients referred to the object side  $C^{(o)}$  given by Eqs. (5) and (11) in the main text. These aberration coefficients are normalized by the values at  $z = z_o$ ; (a) geometrical aberration coefficients and (b) chromatic aberration coefficients.

$z_o$  becomes far from the entrance of the PG, the position of the image plane  $z_i$  becomes far from the GRG exit. In Refs. [6, 7], the negative ion beamlet profiles were measured about 1.0 m downstream of the GRG. This corresponds to  $z_i = 1.25$  m in the present model. From Fig. 7, the value of  $z_i = 1.25$  m is obtained for  $z_o = 3.8$  mm.

### 3.2 Dependence of aberration coefficients on mesh size

The aberration coefficients with the dimension of length  $c^{(i)}$  (given by Eqs. (15) and (16)) are shown in Fig. 8 for  $z_o = 4.0$  mm. In the present calculation model, the

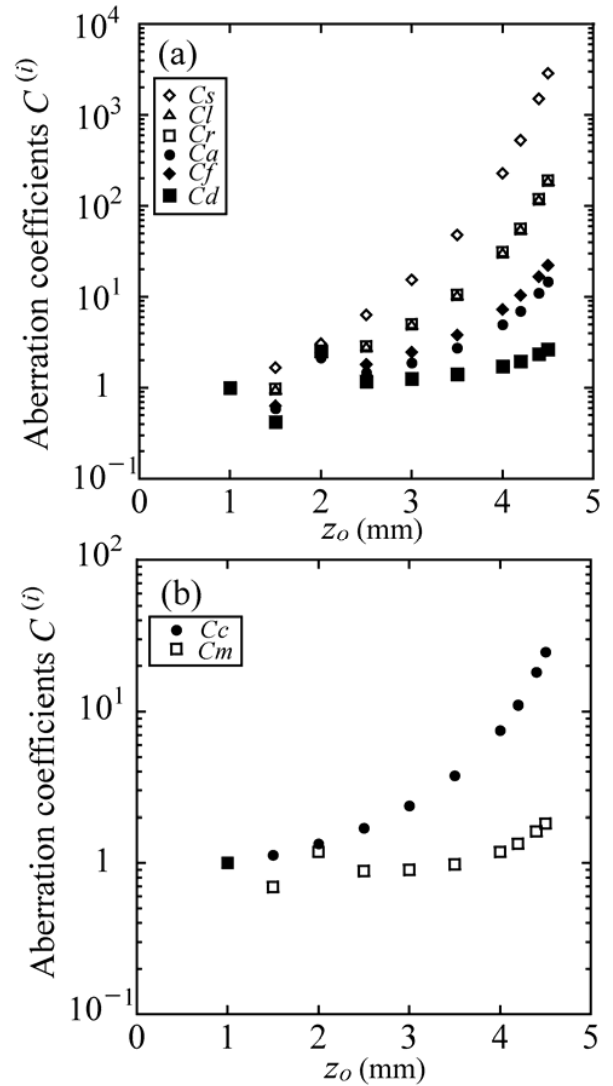


Fig. 5 Aberration coefficients referred to the image side  $C^{(i)}$  given by Eqs. (8) and (13) in the main text. These aberration coefficients are normalized by the values at  $z = z_o$ ; (a) geometrical aberration coefficients and (b) chromatic aberration coefficients.

values of  $\phi_o$  depend on the mesh size  $dh$ , even though the position of the object plane  $z_o$  is fixed. Thus, Fig. 8 compares the aberration coefficients  $c^{(i)}$  for four types of mesh sizes:  $dh = 0.025$  mm ( $\phi_o = 16$  V),  $0.05$  mm ( $\phi_o = 32$  V),  $0.1$  mm ( $\phi_o = 64$  V), and  $0.2$  mm ( $\phi_o = 128$  V). The magnifications  $M$  are almost constant for these four types of mesh sizes.

The deviations of the geometrical aberration coefficients are evaluated to be within 66%. The chromatic aberration coefficients decrease in proportion to  $\sqrt{\phi_o}$ . The chromatic aberration coefficients for  $dh = 0.2$  mm are larger than those for  $dh = 0.025$  mm by a factor of about 2.

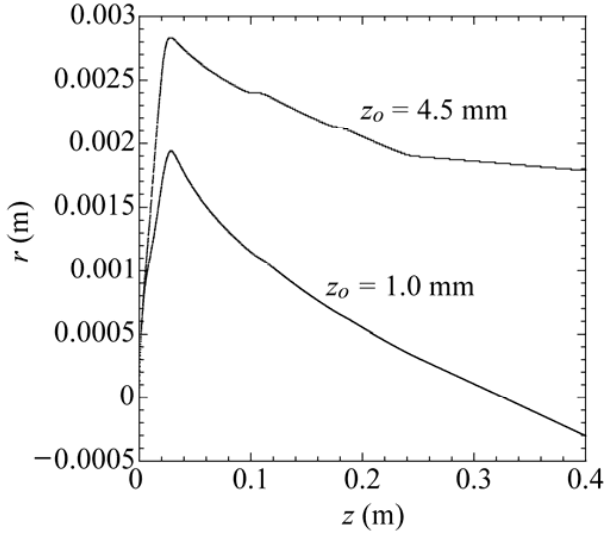


Fig. 6 Comparison of  $h$ -trajectories for  $z_o = 1.0$  mm and  $z_o = 4.5$  mm.

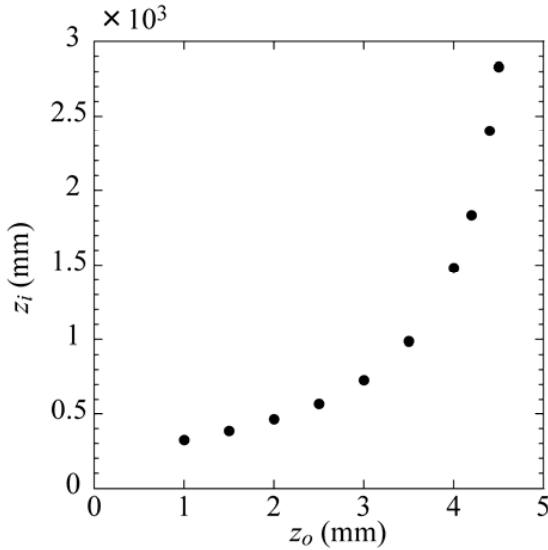


Fig. 7 Position of the image plane  $z_i$  as a function of  $z_o$ .

### 3.3 Contribution of electric field in the extractor/accelerator to the aberration coefficients

The contribution of the electric field at each  $z$  in the extractor/accelerator to the aberration coefficients is shown

$$\frac{\int_{z_o}^{z_i} \sqrt{\frac{\phi}{\phi_o}} \{F_1 h^4 + F_2 h^3 h' + F_3 h^2 h'^2\} dz - \frac{1}{32} \sqrt{\frac{\phi}{\phi_o}} [E_1 h^4 + E_2 h^3 h' + E_3 h^2 h'^2 + E_5 h h'^3]_{z_o}^z}{\int_{z_o}^{z_i} \sqrt{\frac{\phi}{\phi_o}} \{F_1 h^4 + F_2 h^3 h' + F_3 h^2 h'^2\} dz - \frac{1}{32} \sqrt{\frac{\phi}{\phi_o}} [E_1 h^4 + E_2 h^3 h' + E_3 h^2 h'^2 + E_5 h h'^3]_{z_o}^{z_i}}. \tag{24}$$

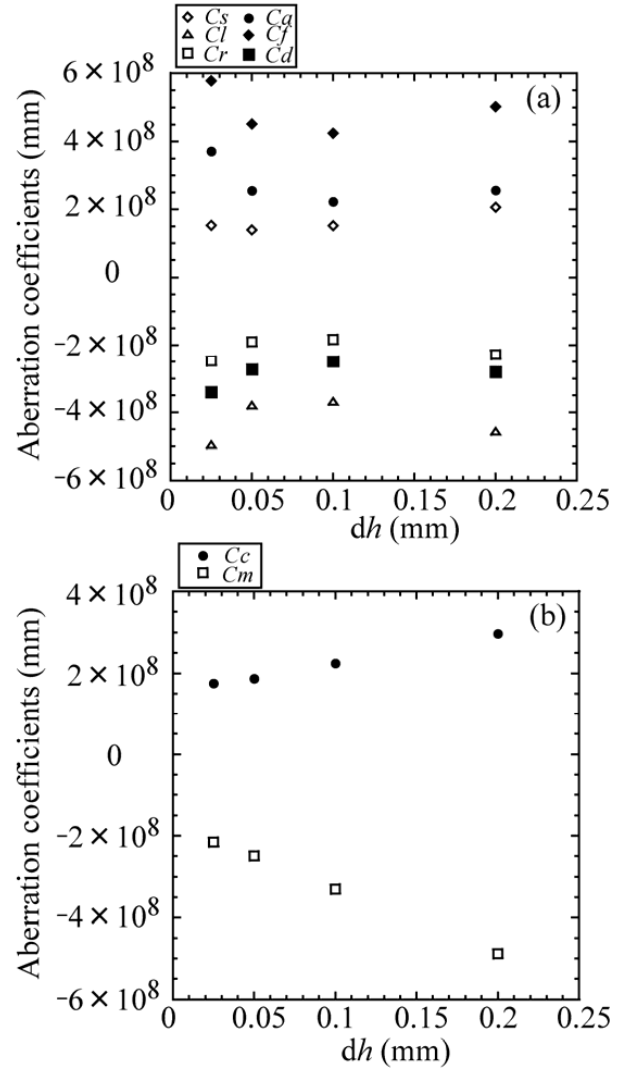


Fig. 8 Aberration coefficients referred to the image side with the dimension of the length  $c^{(i)}$  given by Eqs. (15) and (16) in the main text. The position of the object plane is taken to be  $z_o = 4.0$  mm. Comparison of aberration coefficients  $c^{(i)}$  for four types of mesh sizes:  $dh = 0.025$  mm ( $\phi_o = 16$  V),  $0.05$  mm ( $\phi_o = 32$  V),  $0.1$  mm ( $\phi_o = 64$  V), and  $0.2$  mm ( $\phi_o = 128$  V).

in Fig. 9. The mesh size and position of the object plane are  $dh = 0.025$  mm and  $z_o = 4.0$  mm, respectively. The vertical axis in Fig. 9 is defined such that the aberration coefficients referred to the object side at  $z$  in Eqs. (5) and (11) are normalized by those at the image plane  $z = z_i$ . For example, the normalized spherical aberration coefficient is given as

The normalized aberration coefficients vary largely from the PG to the vicinity of the exit of the EXG, whereas they are almost constant from the A1G to the GRG. This indicates that the electrostatic lenses in the extractor contribute dominantly to the aberration, and the contributions

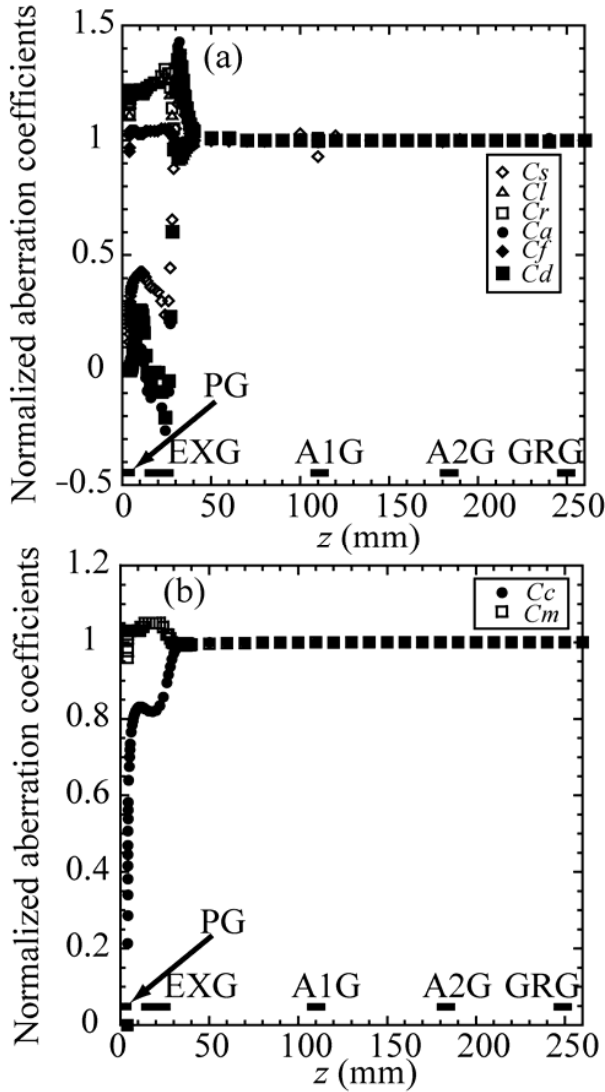


Fig. 9 Contribution of the electric field at each  $z$  in the extractor/accelerator to the aberration coefficients. The mesh size is  $dh = 0.025$  mm. The vertical axis is defined such that the aberration coefficients referred to the object side at  $z$  are normalized by those at the image plane  $z = z_i$ .

from the electrostatic lenses in the accelerator are negligible. This is due to the difference in strength of the convergent electrostatic lenses. As the negative ion beam velocity is much smaller in the extractor than in the accelerator, the space charge effect is larger in the extractor than in the accelerator. Therefore, to suppress the space charge effect, the electrostatic lenses are stronger in the extractor than in the accelerator.

### 3.4 Comparison of electrostatic lens aberrations with negative ion beamlet profile

The aberration due to the electrostatic lenses are compared with the radii of the beam core and beam halo in Refs. [6, 7]. The aberrations for four cases of  $dh = 0.025$  mm ( $\phi_o = 16$  V),  $0.05$  mm ( $\phi_o = 32$  V),  $0.1$  mm ( $\phi_o = 64$  V), and  $0.2$  mm ( $\phi_o = 128$  V) are estimated from the aberration coefficients in Fig. 8.

The overall aberration at the image plane is given as

$$\Delta u(z_i) = c_s u_i'^2 \bar{u}_i' + c_l u_i' \bar{u}_i' \theta_i + c_r u_i'^2 \bar{\theta}_i + c_a \bar{u}_i' \theta_i^2 + c_f u_i' \theta_i \bar{\theta}_i + c_d \theta_i^2 \bar{\theta}_i - (c_c u_i' + c_m \theta_i) \frac{\Delta \phi}{\phi_i}. \quad (25)$$

In the above equation,  $u_i'$  and  $\bar{u}_i'$  correspond to the beam divergence angle of the beam core and beam halo at  $z = z_i$ . This divergence angle of negative ion beamlet is taken to be 5 mrad. From Fig. 3,  $\theta_i$  and  $\bar{\theta}_i$  correspond to the beam divergence angle of the beam core from the principal plane. The calculation results show that the value of  $\theta_i$  or  $\bar{\theta}_i$  is approximately  $4.5 \times 10^{-3}$ , regardless of  $dh$ . The electrostatic potential at the image plane  $\phi_i$  is 406 keV.

The individual and total geometrical aberrations are shown in Table 2. In Refs. [6, 7], the measured  $1/e$  radii for the beam core and halo are 5.8 mm (beam divergence angle: 6 mrad) and 11.5 mm (beam divergence angle: 12 mrad), respectively. Each geometrical aberration is the same order as the radius of the beam halo. However, the geometrical aberrations have positive or negative signs, and thereby cancel each other. The total geometrical aberrations are less than 1 mm. Thus, the total geometrical aberrations are much smaller than the radii of the beam core and halo.

The chromatic aberrations are shown in Fig. 10 as a function of the deviation of the initial kinetic energy  $e\Delta\phi$ . The wide range of  $e\Delta\phi$ , from 0.001 to 100 eV, was surveyed. The chromatic aberrations increase linearly with

Table 2 Individual and total geometrical aberrations due to the electrostatic lenses.

$dh$ (mm)	Spherical aberration $c_s u_i'^2 \bar{u}_i'$ (mm)	Coma $c_l u_i' \bar{u}_i' \theta$ (mm)	Coma $c_r u_i'^2 \bar{\theta}_i$ (mm)	Stigmatism $c_a \bar{u}_i' \theta_i^2$ (mm)	Field curvature $c_f u_i' \theta_i \bar{\theta}_i$ (mm)	Distortion $c_d \theta_i^2 \bar{\theta}_i$ (mm)	Total (mm)
0.025	19.1	-55.0	-27.5	36.6	57.0	-29.8	0.47
0.05	17.4	-43.9	-22.0	27.4	48.5	-27.0	0.36
0.1	19.0	-41.8	-20.9	23.2	44.0	-23.5	0.036
0.2	25.8	-52.9	-26.4	27.6	54.1	-27.9	0.16

Table 3 Individual and total geometrical aberrations due to the space charge effect.

$\alpha_o$	Spherical aberration (mm)	Coma (mm)	Stigmatism (mm)	Field curvature (mm)	Distortion (mm)	Total (mm)
0.1	$-1.72 \times 10^5$	$1.80 \times 10^5$	$-1.87 \times 10^5$	$-3.74 \times 10^5$	$1.95 \times 10^5$	$-3.59 \times 10^5$
0.2	$-7.92 \times 10^5$	$8.25 \times 10^5$	$-8.60 \times 10^5$	$-1.72 \times 10^5$	$8.96 \times 10^5$	$-1.65 \times 10^6$

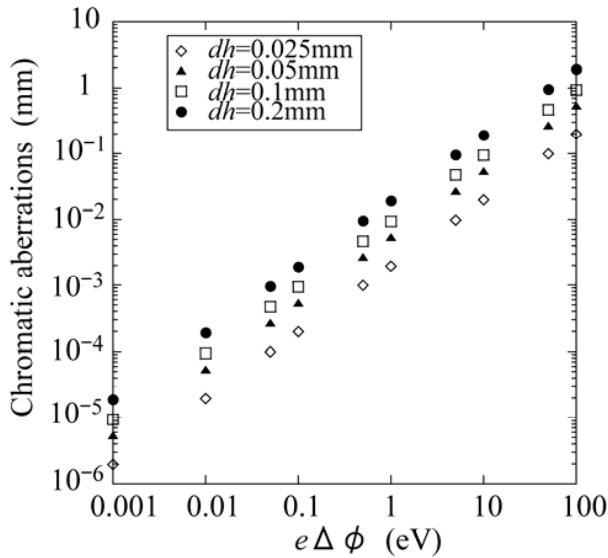


Fig. 10 Chromatic aberrations as a function of the deviation of the initial kinetic energy  $e\Delta\phi$ .

$e\Delta\phi$ . Below  $e\Delta\phi \leq 100$  eV, the chromatic aberrations are less than 2 mm, and negligible compared with the radii of the beam core and halo.

### 3.5 Geometrical aberrations due to space charge effect

The geometrical aberrations due to the space charge effect are summarized in Table 3 for  $dh = 0.1$  mm. From Eq. (23), the  $H^-$  beamlet trajectory or  $R(z)$  depends on the initial beamlet radius  $R_0$ , the incident angle  $\alpha_o$  at the object plane, and the total current  $I$ . In this calculation,  $R_0$  is taken to be 7 mm. For the present calculation model, a realistic  $H^-$  beamlet trajectory will become the minimum beam radius at the position where the negative ion profiles were measured in Refs. [6, 7] ( $z = 1214$  mm in the present model). The values of  $\alpha_o = 0.1$  and  $\alpha_o = 0.2$  are taken because the corresponding  $H^-$  beamlet trajectories  $R(z)$  become minimum around  $z = 1200$  mm. The  $H^-$  beamlet trajectories  $R(z)$  for  $\alpha_o = 0.1$  and  $\alpha_o = 0.2$  are shown in Fig. 11. The current density is  $10 \text{ mA/cm}^2$ , thus, the total current is  $\pi \times 0.7^2 \text{ cm}^2 \times 10 \text{ mA/cm}^2 = 15.4 \text{ mA}$ .

Comparing Tables 2 and 3 show that the geometrical aberrations increase drastically due to the space charge effect. The total aberrations due to the space charge effect

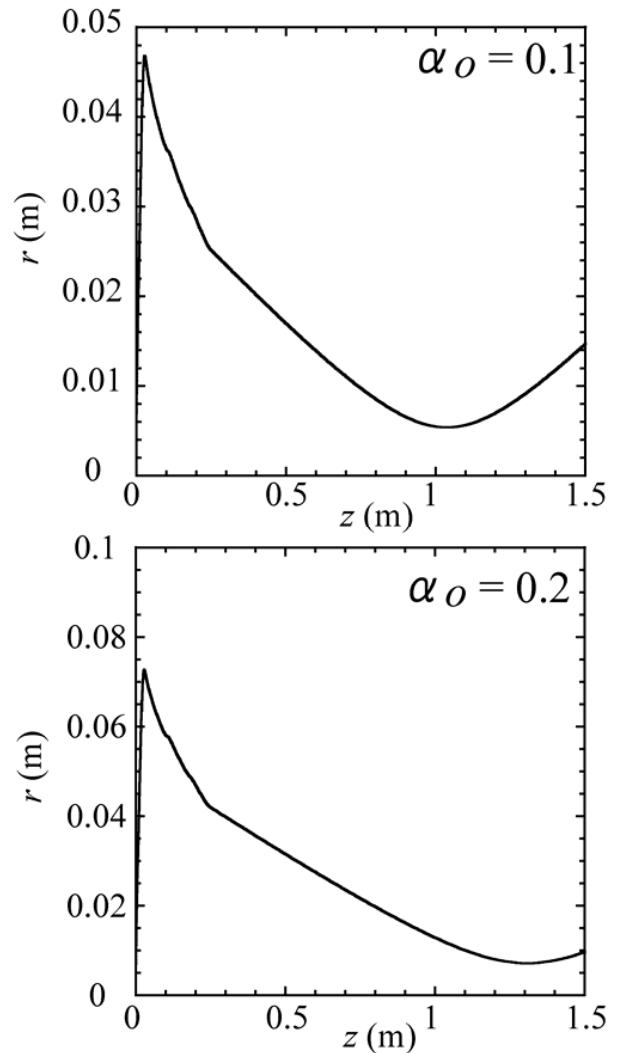


Fig. 11  $H^-$  beamlet trajectories for the incident angles of  $\alpha_o = 0.1$  and  $\alpha_o = 0.2$  with a negative ion current density of  $10 \text{ mA/cm}^2$ .

range from  $10^5$  to  $10^6$  mm of order of magnitude, and are much larger than the radii of the beam core and halo. In reality,  $H^-$  beamlets with such large radii impinge on the grids in the extractor and accelerator. Therefore, in taking account of the aperture radii of the grids, the geometrical aberration is considered to be less than the estimated values in Table 3. However, the results indicate that the space charge effect is an important factor for aberrations or halo in a negative ion accelerator.

### 4. Summary

The aberrations of the negative ion source/accelerator for neutral beam injector were theoretically estimated. The aberrations are considered to be caused by the electrostatic lenses, magnetic lenses, space charge effect, and shape of the beam-plasma boundary. In this study, the aberrations due to the electrostatic lenses and the space charge effect were investigated, and compared with the radii of the beam core and halo obtained in the H<sup>-</sup> beamlet profile measurements with the 400 keV negative ion accelerator. From this measurement, the 1/e radii of the beam core and beam halo were evaluated to be 5.8 and 11.5 mm, respectively. In the present calculation, the beam energy was taken to be 406 keV, and the electrostatic lenses were similar to those of the 400 keV negative ion accelerator. The aberration coefficients were numerically calculated using the eikonal method, which is conventionally used in electron optics.

The calculation results are summarized as follows:

- 1) The electrostatic lenses in the extractor dominantly contribute to the aberration coefficients.
- 2) Based on the assumption that the divergence angle of the beam core is 5 mrad, the aberration due to the electrostatic lenses is less than a few millimeters, i.e., less than the radii of the beam core and halo. Therefore, the aberration due to the electrostatic lenses in the extractor/accelerator is not the reason for the beam halo.
- 3) With a negative current density of 10 mA/cm<sup>2</sup>, the geometrical aberrations due to the space charge are estimated to be from 10<sup>5</sup> to 10<sup>6</sup> mm of order of magnitude. Unlike the aberration from the electrostatic lenses, the geometrical aberration due to the space charge is much larger than the radii of the beam core and beam halo. Although the aperture radii of the grids are not taken into account in this estimation, the results indicate that the space charge effect is an important factor in the aberration or beam halo in the negative ion accelerator.

### Appendix. Eikonal Method

Let us consider the motion of a charged particle with an electric charge  $e$  and mass  $m$ . In the eikonal method, the variational function  $F$  satisfies

$$\Delta \int F dz = 0, \tag{A1}$$

where

$$\begin{aligned}
 F &= \sqrt{\hat{\phi}(1+x'^2+y'^2)} - \eta(A_x x' + A_y y' + A_z), \\
 \eta &= \sqrt{\frac{e}{2m}}, \\
 \hat{\phi} &= \phi(1 + \varepsilon\phi), \\
 \varepsilon &= \frac{e}{2mc^2}.
 \end{aligned} \tag{A2}$$

In Eq. (A2),  $c$  is the velocity of light. In the absence of a magnetic field, the magnetic vector potential is zero, i.e.,

$A_x = A_y = A_z = 0$ . In the non-relativistic approximation,  $\varepsilon$  is zero. Consider an optical system without a magnetic field, and the non-relativistic case. Moreover, the space charge effect is not taken into account.

First we deal with the geometrical aberration. From Eq. (A1), the Lagrange equation of motion is given as

$$\frac{d}{dz} \left( \frac{\partial F}{\partial \bar{u}'} \right) - \frac{\partial F}{\partial \bar{u}} = 0, \tag{A3-1}$$

$$\frac{d}{dz} \left( \frac{\partial F}{\partial u'} \right) - \frac{\partial F}{\partial u} = 0. \tag{A3-2}$$

The characteristic function  $F$  can be expanded as follows:

$$F = F_0 + F_2 + F_4 + \dots, \tag{A4}$$

$$F_0 = \sqrt{\phi},$$

$$F_2 = \frac{\sqrt{\phi}}{2} \left( u' \bar{u}' - \frac{\phi''}{4\phi} \right),$$

$$\begin{aligned}
 F_4 &= -\sqrt{\phi} \left\{ \frac{1}{128} \left( \frac{\phi''^2 - \phi^{(4)}\phi}{\phi^2} \right) (u\bar{u})^2 + \frac{\phi''}{16\phi} (u\bar{u}u'\bar{u}') \right. \\
 &\quad \left. + \frac{1}{8} (u'\bar{u}')^2 \right\}.
 \end{aligned} \tag{A5}$$

In Eq. (A5),  $F_2$  corresponds to the paraxial ray and  $F_4$  corresponds to the aberration. When we neglect the aberration term  $F_4$ , Eq. (A3-1) is given as

$$\frac{d}{dz} \left( \frac{\partial(F_0 + F_2)}{\partial \bar{u}'} \right) - \frac{\partial(F_0 + F_2)}{\partial \bar{u}} = 0. \tag{A6}$$

By substituting Eq. (A5) into (A6), we obtain

$$u'' + \frac{\phi'}{2\phi} u' + \frac{\phi''}{4\phi} u = 0. \tag{A7}$$

Equation (A7) is the paraxial equation, and the solution corresponds to the paraxial ray  $u_G$ .

In estimating the aberration, we should take  $F_4$  into account for Eq. (A3-1):

$$\frac{d}{dz} \left( \frac{\partial(F_0 + F_2 + F_4)}{\partial \bar{u}'} \right) - \frac{\partial(F_0 + F_2 + F_4)}{\partial \bar{u}} = 0. \tag{A8}$$

Equation (A8) can be written as

$$\frac{d}{dz} \left( \frac{\partial F_2}{\partial \bar{u}'} \right) - \frac{\partial F_2}{\partial \bar{u}} = \frac{\partial F_4}{\partial \bar{u}} - \frac{d}{dz} \left( \frac{\partial F_4}{\partial \bar{u}'} \right). \tag{A9}$$

The solution of Eq. (A9) will be written as  $u = u_G + u_3$ , where  $u_G$  and  $u_3$  are the paraxial ray  $u_G$  and geometrical aberration, respectively. Note that  $u_3$  is the third order term. By substituting  $u = u_G + u_3$  into the left side, we obtain

$$\begin{aligned}
 \frac{d}{dz} \left( \frac{\partial F_2}{\partial \bar{u}'} \right) - \frac{\partial F_2}{\partial \bar{u}} &= \frac{\sqrt{\phi}}{2} \left\{ (u_G + u_3)'' + \frac{\phi'}{2\phi} (u_G + u_3)' \right. \\
 &\quad \left. + \frac{\phi''}{4\phi} (u_G + u_3) \right\}.
 \end{aligned} \tag{A10}$$

Since  $u_G$  is the solution of the paraxial equation (A7), Eq. (A10) can be transformed into

$$\frac{d}{dz} \left( \frac{\partial F_2}{\partial \bar{u}'} \right) - \frac{\partial F_2}{\partial \bar{u}} = \frac{\sqrt{\phi}}{2} \left( u_3'' + \frac{\phi'}{2\phi} u_3' + \frac{\phi''}{4\phi} u_3 \right). \quad (A11)$$

On the other hand, let us define the right side of Eq. (A9) as

$$W = W(u, \bar{u}, u', \bar{u}', u'', \bar{u}'') = \frac{\partial F_4}{\partial \bar{u}} - \frac{d}{dz} \left( \frac{\partial F_4}{\partial \bar{u}'} \right). \quad (A12)$$

The right side of Eq. (A9)  $W(u, \bar{u}, u', \bar{u}', u'', \bar{u}'')$  can be expanded in Taylor's series:

$$W(u, \bar{u}, u', \bar{u}', u'', \bar{u}'') = W(u_G, \bar{u}_G, u'_G, \bar{u}'_G, u''_G, \bar{u}''_G) + \frac{\partial W}{\partial \bar{u}} \Big|_G \bar{u}_3 + \frac{\partial W}{\partial u} \Big|_G u_3 + \frac{\partial W}{\partial \bar{u}'} \Big|_G \bar{u}'_3 + \frac{\partial W}{\partial u'} \Big|_G u'_3 + \frac{\partial W}{\partial \bar{u}''} \Big|_G \bar{u}''_3 + \frac{\partial W}{\partial u''} \Big|_G u''_3. \quad (A13)$$

In Eq. (A11),  $\frac{\partial W}{\partial \bar{u}} \Big|_G, \frac{\partial W}{\partial u} \Big|_G, \frac{\partial W}{\partial \bar{u}'} \Big|_G, \frac{\partial W}{\partial u'} \Big|_G, \frac{\partial W}{\partial \bar{u}''} \Big|_G, \frac{\partial W}{\partial u''} \Big|_G$  denote  $\frac{\partial W}{\partial \bar{u}} \Big|_{\bar{u}=\bar{u}_G}, \frac{\partial W}{\partial u} \Big|_{u=u_G}, \frac{\partial W}{\partial \bar{u}'} \Big|_{\bar{u}'=\bar{u}'_G}, \frac{\partial W}{\partial u'} \Big|_{u'=u'_G}, \frac{\partial W}{\partial \bar{u}''} \Big|_{\bar{u}''=\bar{u}''_G}, \frac{\partial W}{\partial u''} \Big|_{u''=u''_G}$ , respectively. In the third order approximation of the aberration, the terms  $\frac{\partial W}{\partial \bar{u}} \Big|_G \bar{u}_3, \frac{\partial W}{\partial u} \Big|_G u_3, \frac{\partial W}{\partial \bar{u}'} \Big|_G \bar{u}'_3, \frac{\partial W}{\partial u'} \Big|_G u'_3, \frac{\partial W}{\partial \bar{u}''} \Big|_G \bar{u}''_3, \frac{\partial W}{\partial u''} \Big|_G u''_3$  can be negligible, since  $u_3$  is the third order term. Thus, we obtain

$$W(u, \bar{u}, u', \bar{u}', u'', \bar{u}'') = W(u_G, \bar{u}_G, u'_G, \bar{u}'_G, u''_G, \bar{u}''_G). \quad (A14)$$

Note that from Eq. (A14), mathematically,  $u, \bar{u}, u', \bar{u}', u'', \bar{u}''$  on the right side of Eqs. (A9) or (A12) are equivalently replaced with  $u_G, \bar{u}_G, u'_G, \bar{u}'_G, u''_G, \bar{u}''_G$ . Thus, we define  $F_{4G}$  as  $F_{4G} = F_4(u_G, \bar{u}_G, u'_G, \bar{u}'_G)$ , and in the third approximation of the aberration, we obtain

$$W(u, \bar{u}, u', \bar{u}', u'', \bar{u}'') = \frac{\partial F_{4G}}{\partial \bar{u}_G} - \frac{d}{dz} \left( \frac{\partial F_{4G}}{\partial \bar{u}'_G} \right). \quad (A15)$$

From Eqs. (A11) and (A15), the ray equation for the aberration is given as

$$\frac{\sqrt{\phi}}{2} \left( u_3'' + \frac{\phi'}{2\phi} u_3' + \frac{\phi''}{4\phi} u_3 \right) = \frac{\partial F_{4G}}{\partial \bar{u}_G} - \frac{d}{dz} \left( \frac{\partial F_{4G}}{\partial \bar{u}'_G} \right). \quad (A16)$$

We set the solution of Eq. (A16) as

$$u_3 = \alpha g + \beta h. \quad (A17)$$

Moreover, we add the condition of

$$\alpha' g + \beta' h = 0. \quad (A18)$$

The initial condition for the aberration is set at  $u_3(z_0) = u_3'(z_0) = 0$ . By applying Lagrange's method of undetermined multipliers to Eq. (A17), we obtain

$$\alpha = \left[ \frac{2}{\phi_0} \frac{\partial F_{4G}}{\partial \bar{u}'_G} h \right]_{z_0}^{z_1} - \frac{2}{\sqrt{\phi_0}} \int_{z_0}^z \left\{ \frac{\partial F_{4G}}{\partial \bar{u}_G} h + \frac{\partial F_{4G}}{\partial \bar{u}'_G} h' \right\} dz, \quad (A19)$$

$$\beta = \left[ -\frac{2}{\phi_0} \frac{\partial F_{4G}}{\partial \bar{u}'_G} g \right]_{z_0}^{z_1} + \frac{2}{\sqrt{\phi_0}} \int_{z_0}^z \left\{ \frac{\partial F_{4G}}{\partial \bar{u}_G} g + \frac{\partial F_{4G}}{\partial \bar{u}'_G} g' \right\} dz.$$

The initial condition for the paraxial ray is set to be  $u_G(z_0) = u_0, u'_G(z_0) = u'_0$ . The paraxial ray can be expressed as

$$u_G(z) = u_0 g(z) + u'_0 h(z). \quad (A20)$$

Thus, we obtain

$$u'_G(z) = u_0 g'(z) + u'_0 h'(z), \quad (A21)$$

$$\bar{u}_G(z) = \bar{u}_0 g(z) + \bar{u}'_0 h(z),$$

$$\bar{u}'_G(z) = \bar{u}_0 g'(z) + \bar{u}'_0 h'(z).$$

From Eq. (A21), we can obtain the following relations:

$$\frac{\partial F_{4G}}{\partial \bar{u}'_0} = \frac{\partial F_{4G}}{\partial \bar{u}_G} h + \frac{\partial F_{4G}}{\partial \bar{u}'_G} h', \quad (A22)$$

$$\frac{\partial F_{4G}}{\partial \bar{u}_0} = \frac{\partial F_{4G}}{\partial \bar{u}_G} g + \frac{\partial F_{4G}}{\partial \bar{u}'_G} g'.$$

By substituting Eq. (A22) into Eq. (A19), we obtain

$$\alpha = \left[ \frac{2}{\phi_0} \frac{\partial F_{4G}}{\partial \bar{u}'_G} h \right]_{z_0}^{z_1} - \frac{2}{\sqrt{\phi_0}} \frac{\partial}{\partial \bar{u}'_0} \int_{z_0}^z F_{4G} dz, \quad (A23)$$

$$\beta = \left[ -\frac{2}{\phi_0} \frac{\partial F_{4G}}{\partial \bar{u}'_G} g \right]_{z_0}^{z_1} + \frac{2}{\sqrt{\phi_0}} \frac{\partial}{\partial \bar{u}_0} \int_{z_0}^z F_{4G} dz.$$

The values of  $g(z)$  and  $h(z)$  at the image plane  $z = z_1$  are given by  $g(z_1) = M, h(z_1) = 0$  (see Fig. 3). Thus, with Eq. (A17), the aberration at  $z = z_1$  is expressed as

$$u_3(z_1) = \alpha(z_1)g(z_1) + \beta(z_1)h(z_1) = M\alpha(z_1). \quad (A24)$$

By replacing  $u, \bar{u}, u', \bar{u}'$  in the term  $F_4$  with the paraxial solutions  $u_G, \bar{u}_G, u'_G, \bar{u}'_G$ , and substituting Eqs. (A20) and (A21) into Eq. (A23), we obtain

$$\alpha = \left[ \frac{2}{\phi_0} \frac{\partial F_{4G}}{\partial \bar{u}'_G} h \right]_{z_0}^{z_1} + C_s^{(0)} u_0'^2 \bar{u}_0'^2 + C_1^{(0)} u_0' \bar{u}_0' u_0 + C_r^{(0)} u_0'^2 \bar{u}_0 + C_a^{(0)} u_0'^2 \bar{u}_0' + C_f^{(0)} u_0 \bar{u}_0 u_0' + C_d^{(0)} u_0^2 \bar{u}_0, \quad (A25)$$

where the coefficients of  $C_s^{(0)}, C_1^{(0)}, C_r^{(0)}, C_a^{(0)}, C_f^{(0)}, C_d^{(0)}$  are given as follows:

$$C_s^{(0)} = \int_{z_0}^z \sqrt{\frac{\phi}{\phi_0}} \left\{ \frac{1}{32} \left( \frac{\phi''^2 - \phi^{(4)}\phi}{\phi^2} \right) h^4 + \frac{\phi''}{4\phi} h^2 h'^2 + \frac{1}{2} h'^4 \right\} dz,$$

$$\begin{aligned} \frac{1}{2}C_1^{(o)} = C_r^{(o)} &= \int_{z_o}^{\infty} \sqrt{\frac{\phi}{\phi_o}} \left\{ \frac{1}{32} \left( \frac{\phi''^2 - \phi^{(4)}\phi}{\phi^2} \right) gh^3 \right. \\ &\quad \left. + \frac{\phi''}{8\phi} (gh)'hh' + \frac{1}{2}g'h'^3 \right\} dz, \\ C_a^{(o)} &= \int_{z_o}^{\infty} \sqrt{\frac{\phi}{\phi_o}} \left\{ \frac{1}{32} \left( \frac{\phi''^2 - \phi^{(4)}\phi}{\phi^2} \right) g^2h^2 \right. \\ &\quad \left. + \frac{\phi''}{4\phi} gg'hh' + \frac{1}{2}g'^2h'^2 \right\} dz, \\ C_f^{(o)} &= \int_{z_o}^{\infty} \sqrt{\frac{\phi}{\phi_o}} \left\{ \frac{1}{32} \left( \frac{\phi''^2 - \phi^{(4)}\phi}{\phi^2} \right) g^2h^2 \right. \\ &\quad \left. + \frac{\phi''}{8\phi} (gh' + g'h)^2 + g'^2h'^2 \right\} dz, \\ C_d^{(o)} &= \int_{z_o}^{\infty} \sqrt{\frac{\phi}{\phi_o}} \left\{ \frac{1}{32} \left( \frac{\phi''^2 - \phi^{(4)}\phi}{\phi^2} \right) g^3h \right. \\ &\quad \left. + \frac{\phi''}{8\phi} gg'(gh)' + \frac{1}{2}g'^3h' \right\} dz. \end{aligned} \quad (A26)$$

The first term on the right side of Eq. (A25) becomes zero because  $h(z_o) = h(z_i) = 0$ . Therefore, the aberration is given by

$$\begin{aligned} u_3(z_i) &= M \left( C_s^{(o)} u_o'^2 \bar{u}_o' + C_1^{(o)} u_o' \bar{u}_o' u_o + C_r^{(o)} u_o'^2 \bar{u}_o \right. \\ &\quad \left. + C_a^{(o)} u_o'^2 \bar{u}_o' + C_f^{(o)} u_o \bar{u}_o u_o' + C_d^{(o)} u_o^2 \bar{u}_o \right). \end{aligned} \quad (A27)$$

The chromatic aberration  $u_c$  can be calculated with a similar procedure, and is given by Eqs. (10) and (11) in the main text.

[1] T. Inoue *et al.*, Rev. Sci. Instrum. **71**, 744 (2000).  
 [2] ITER EDA Final Design Report, ITER technical basis, Plant Description Document (PDD), G A0 FDR 1 01-07-13 R1.0, IAEA EDA documentation No. 24, 2002.  
 [3] T. Inoue *et al.*, Rev. Sci. Instrum. **75**, 1819 (2004).  
 [4] M. Taniguchi *et al.*, Rev. Sci. Instrum. **77**, 03A514 (2006).  
 [5] A.J.T. Holmes and M.P.S. Nightingale, Rev. Sci. Instrum. **57**, 2402 (1986).

[6] K. Miyamoto *et al.*, in Proceeding of the joint meeting of the 7th International Symposium on the Production and Neutralization of Negative Ions and Beams and 6th European Workshop on the Production and Application of Light Negative Ions (Upton, New York, Oct. 23 ~ 27, 1995), AIP Conference Proceedings 380 (1996) p. 390.  
 [7] K. Miyamoto *et al.*, in Proceedings of the 17th IEEE/NPSS Symposium on Fusion Engineering (San Diego, California, Oct. 6 ~ 10, 1997), vols.1 and 2 (1998) p. 1067.  
 [8] R.S. Hemsworth *et al.*, Rev. Sci. Instrum. **67**, 1120 (1996).  
 [9] P.W. Hawkes, *Magnetic Electron Lenses*, Chapt. 1 (Springer Verlag, 1982).  
 [10] F.H. Read, J. Phys. E **2**, 165 (1969).  
 [11] F.H. Read, J. Phys. E **3**, 127 (1970).  
 [12] E. Munro, Optik **39**, 450 (1974).  
 [13] A. Renau and D.W.O. Heddle, J. Phys. E **19**, 288 (1986).  
 [14] S. Naganachi *et al.*, Rev. Sci. Instrum. **67**, 2351 (1996).  
 [15] T. Tang, J. Orloff and L. Wang, J. Vac. Sci. Technol. B **14**, 80 (1996).  
 [16] K. Sakaguchi and T. Sekine, J. Vac. Sci. Technol. B **16**, 2462 (1998).  
 [17] K. Kanaya, H. Kawakatsu and H. Yamazaki, Br. J. Appl. Phys. **16**, 991 (1965).  
 [18] W. Glaser, Elektronen und Ionenoptik. Handbuch der Physik **33**, 123 (1956).  
 [19] K. Ura, *Electron and Ion Beam Optics*, Chapt. 15 (Kyouritsu Shuppan CO., LTD., 1994) [in Japanese].  
 [20] S. Takashima, *Basis of Theory and Simulation for Electron Optics* [JEOL textbook in Japanese, unpublished].  
 [21] P.W. Hawkes, Adv. Electronics and Electron Physics, Suppl. **7** (Academic Press Inc., June, 1970).  
 [22] M. Kuriyama *et al.*, Fusion Sci. Technol. **42**, 410 (2002).  
 [23] Y. Okumura *et al.*, Rev. Sci. Instrum. **67**, 1018 (1996).  
 [24] K. Miyamoto *et al.*, in Proceedings of the 18th Symposium on Fusion Technology (Karlsruhe, 1994), Elsevier, Amsterdam, vol.1 (1995) p.625.  
 [25] M. Hanada *et al.*, Rev. Sci. Instrum. **69**, 947 (1998).  
 [26] T. Morishita *et al.*, Rev. Sci. Instrum. **73**, 1064 (2002).  
 [27] M. Hanada *et al.*, Rev. Sci. Instrum. **77**, 03A515 (2006).  
 [28] A. Hatayama, Rev. Sci. Instrum. **79**, 02B901 (2008).  
 [29] R. Becker, Rev. Sci. Instrum. **67**, 1132 (1996).  
 [30] O.I. Seman, Radiotech. Electron. **3**, 402, 1702 (1958).  
 [31] P.W. Hawkes, Optik **24**, 252 (1966/67).  
 [32] P.W. Hawkes, Optik **24**, 257 (1966/67).